



## Drug-loaded balloon with built-in NIR controlled tip-separable microneedles for long-effective arteriosclerosis treatment

Li Huang<sup>a,b</sup>, Huaqiang Fang<sup>a</sup>, Teng Zhang<sup>a</sup>, Binbin Hu<sup>b</sup>, Shichen Liu<sup>a</sup>, Fanzhen Lv<sup>a</sup>, Zhaoxia Zeng<sup>c</sup>, Huijie Liu<sup>b</sup>, Weimin Zhou<sup>a,\*</sup>, Xiaolei Wang<sup>b,d,\*\*</sup>

<sup>a</sup> Department of Vascular Surgery, The Second Affiliated Hospital of Nanchang University, Nanchang University, Nanchang, Jiangxi, 330006, PR China

<sup>b</sup> The National Engineering Research Center for Bioengineering Drugs and the Technologies, Institute of Translational Medicine, Nanchang University, Nanchang, Jiangxi, 330088, PR China

<sup>c</sup> Department of Radiology, The Second Affiliated Hospital of Nanchang University, Nanchang University, Nanchang, Jiangxi, 330006, PR China

<sup>d</sup> School of Chemistry and Chemical Engineering, Nanchang University, Nanchang, Jiangxi, 330088, PR China

### ARTICLE INFO

#### Keywords:

Photothermal responsive  
Drug delivery  
Microneedles  
Atherosclerosis  
Drug-eluting balloon

### ABSTRACT

Drug-eluting balloon (DEB) angioplasty has emerged as an effective treatment for cardiovascular and cerebrovascular diseases. However, distal embolism and late lumen restenosis could be caused by drug loss during DEB handling and rapid drug metabolism. Here, a drug-loaded balloon equipped with tip-separable microneedles on the balloon surface (MNDLB) was developed. Inbuilt near-infrared (NIR) ring laser inside the catheter inner shaft was introduced to activate the biodegradable microneedle tips for the first time. The drug-loaded tips thus could be embedded in the vasculature and then released antiproliferative drug – paclitaxel slowly *via* polymer degradation for more than half a year. A significant increase in drug delivery efficiency and superior therapeutic effectiveness compared with the standard DEB were demonstrated using an atherosclerosis rabbit model.

### 1. Introduction

In the past decade, the death number of cardiovascular and cerebrovascular diseases (CCVDs) has increased by 12.5%, accounting for about 1/3 of the total global deaths [1,2]. Arteriosclerosis (AS) is at the root of the most life-threatening CCVDs, which eventually advances to coronary heart disease, ischemic stroke or peripheral artery atherosclerotic occlusion [3]. For severely stenotic or obstructed blood vessels, operations are commonly required, which primarily encompass artery reconstruction surgery and minimally invasive percutaneous transluminal angioplasty (PTA) [4]. In particular, drug-eluting balloon (DEB) angioplasty, one of the crucial PTA against CCVDs, restores blood flow by dilating the stenotic vessel and the surrounding muscular wall. Meanwhile, anti-proliferative agents coated on DEB are stamped to the vascular wall to inhibit subsequent intimal hyperplasia [5]. At present, DEB angioplasty is recommended exclusively in the situations where stents are not suitable, such as in-stent restenosis, small vessel lesions and bifurcation lesions [6,7].

Despite its benefits, the present DEB also has some intrinsic defects. Firstly, the drug delivery efficiency of DEB is generally low due to undesired considerable drug loss during angioplasty, because the adhesion of the balloon and drug coating is weakened for optimal drug transfer to the target tissue [8,9]. Scholars Svea Petersen et al. reported the drug loss of three coating formulations – cetpyrsal/paclitaxel (PTX), hyaluronic acid (HA)/PTX and polyvinylpyrrolidone (PVP)/PTX to be about 28%, 21% and 39%, respectively [10]. Involuntary drug loss not only leads to different drug dosages in the target regions, contributing to the variations of therapeutic outcome, but also causes downstream vascular embolism and deterioration of the disease [11,12]. Secondly, intimal hyperplasia and negative remodeling of the vessels last for several months after DEB dilatation, while the rapid metabolism of drugs stamped to the vessel wall can't work for such long, resulting in late intraluminal restenosis [13,14].

Although great advance has been made to optimize drug release, current DEBs still have limitations in terms of drug transfer efficacy and drug loss [15]. Giving these objects and challenges, microneedle (MN)

Peer review under responsibility of KeAi Communications Co., Ltd.

\* Corresponding author.

\*\* Corresponding author. The National Engineering Research Center for Bioengineering Drugs and the Technologies, Institute of Translational Medicine, Nanchang University, Nanchang, Jiangxi, 330088, PR China.

E-mail addresses: [drzwm@sina.com](mailto:drzwm@sina.com) (W. Zhou), [wangxiaolei@ncu.edu.cn](mailto:wangxiaolei@ncu.edu.cn) (X. Wang).

<https://doi.org/10.1016/j.bioactmat.2022.11.015>

Received 12 August 2022; Received in revised form 24 October 2022; Accepted 22 November 2022

2452-199X/© 2022 The Authors. Publishing services by Elsevier B.V. on behalf of KeAi Communications Co. Ltd. This is an open access article under the CC BY-NC-ND license (<http://creativecommons.org/licenses/by-nc-nd/4.0/>).

patches, an extensively researched drug delivery device, especially the separable MN, may be a suitable solution just as it has been applied transdermally [16–19]. To improve the efficacy and accuracy of MNs-based drug delivery in blood vessel environment, the photothermal tip-separable microneedles drug-loaded balloon (MNDLB) was proposed in this study. Rather than the regular DEB with drug sprayed on the surface that was easily washed off without a strong bond to the balloon surface (Fig. 1A–C), the antiproliferative drug was totally encapsulated in the MN tips of our designed MNDLB and delivered into the vessel wall as MN inserted the luminal lesion. A ring-laser fiber was then introduced into the catheter's inner shaft, which was withdrawn slowly and emitted 808 nm near-infrared (NIR) simultaneously to heat and melt the phase-change material lauric acid (LA) in the MN tips. After that, the molten LA transformed into a solid state again, resulting in a weakened bond between the MN tip and the base. Thus, only a mild shear force pulling the balloon catheter by hand was able to detach the tips from the bases, leaving the entire drug-loaded tips remained in the lesion tissue. Subsequently, the embedded tips sustainably released the drug by the degradation of polycaprolactone (PCL)/poly(lactic-co-glycolic acid) (PLGA) (Fig. 1D–F). Theoretically, this rapidly photothermal tip-separable MNDLB, providing optimal drug transfer and long-term restenosis inhibition, is expected to become a promising solution of atherosclerosis.

## 2. Materials and methods

### 2.1. Materials

Balloons (APT Medical Inc., China), DEBs (Lifetech Scientific Co., Ltd, China), pressure pump (Allwell, IS-30-A, USA) and contrast agent Onepike (350 mg/L, GE Co., USA) were kindly provided by the Cardiac Intervention Unit of the Second Affiliated Hospital of Nanchang University. Polydimethylsiloxane (PDMS) MN molds were customized from Microchip Pharmaceutical Technology (Zhejiang, China, samples specifications were shown in Fig. S1). PTX (99%), LA (99%), PCL (Mw = 36,000–45,000), PLGA (LA:GA = 50:50, Mw = 24,000–38,000), polyvinyl alcohol (PVA, Mw = 89,000–98,000, hydrolysis >99%), dichloromethane standard, docetaxel (>99%), Rhodamine B (RhB) and alcohol soluble melanin were purchased from Aladdin Co., Ltd, Shanghai, China. Curable resin PCLMA (containing photoinitiator TPO-L) was purchased from Engineering for Life (Suzhou, China).

### 2.2. Fabrication of two-section MNs patch

First, the solution of drug-loaded tips was prepared: 0.125 g PCL and 0.125 g PLGA were co-dissolved in 2 mL dichloromethane; 0.2 g PTX and

0.05 g LA were co-dissolved in 2 mL ethanol; these two fluids were mixed together with additional 1 mL deionized (DI) water to slow the solvent evaporation. Then, 20  $\mu$ L mixing solution was cast onto the PDMS MN mold, vacuumed ( $-1$  kg/cm<sup>2</sup>) for 2 min to fill the MN cavities completely, and dried in a vacuum drying oven at 35 °C for 48 h. This process was repeated one more time to get more drug loading. Next, MN bases were fabricated: 20  $\mu$ L curable resin was cast onto the PDMS mold when drug-tips was finished, then vacuumed ( $-1$  kg/cm<sup>2</sup>) for 2 min, and solidified under 405 nm blue light for 1 min. Finally, the PDMS mold was carefully demolded to get the two-section MNs patch.

### 2.3. Fabrication of MNDLB

MN array was transferred to the curved surface of the balloon referring to “conformal transfer modeling method” [20]: two-section MNs were fabricated as described above, and the PDMS mold was then wrapped around the inflated balloon precisely; next, the entire apparatus was exposed to blue-light for 2 min to fix the MN array onto the surface of the DEB; finally, PDMS was carefully demolded to get a two-section MNDLB.

### 2.4. Characterizations of MNs

MNs prepared in this study were characterized using scanning electron microscopy (SEM), Fourier transform infrared spectroscopy (FTIR), differential scanning calorimetry (DSC), and inverted fluorescence microscopy. A SEM ( $\Sigma$ -300 Zeiss AG, Germany) was used to image the morphology of the cross-sections of MNs with or without photothermal stimulation. A Nicolet iS20 (Thermo, U.S.A.) FTIR spectroscopy was used to characterize the drug-loaded tip and its components. All FTIR spectra were collected at 1024 scans with a spectral resolution of 4 cm<sup>-1</sup>. All collected spectra were analyzed using OriginPro 2018C software. DSC measurements were performed on a DSC Q20 V24.10 Build 122 instrument in this study to characterize LA and MNs tip. For this characterization, a sample weighing 5–10 mg was sealed in an aluminum pan and heated from 20 °C to 100 °C at a scan rate of 5 °C/min. All DSC measurements were carried out under nitrogen gas at a flow rate of 50 mL/min. Fluorescein 7-amino-4-methyl coumarin (AMC)-labeled LA (AMC-LA, NJPeptide Biotechnology Co. Ltd, China) was used to test the distribution of LA. MNs were sectioned to a thickness of 4  $\mu$ m and pictured with inverted fluorescence microscopy (BCD-606WKPZM, Olympus, Japan).

### 2.5. Preparation of vascular phantoms

Vascular phantoms with different stiffness were prepared according

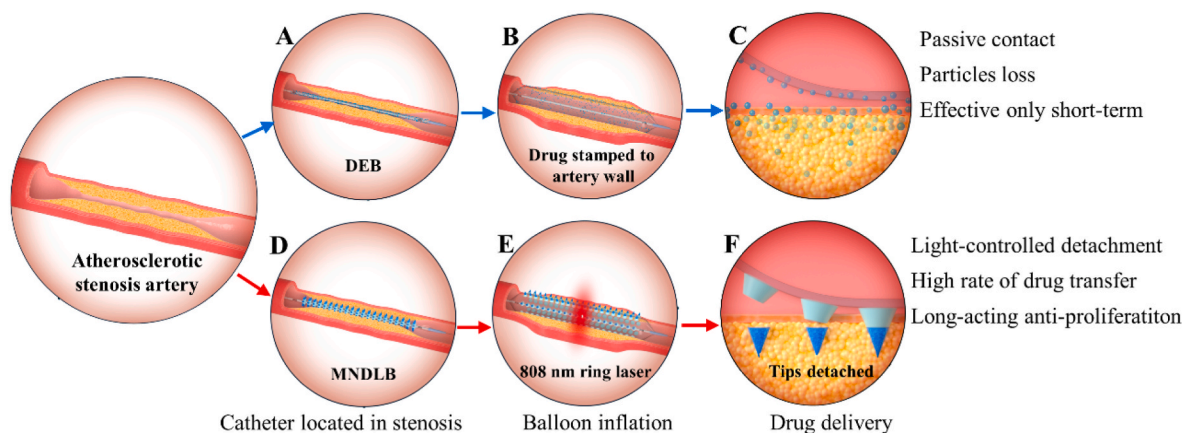


**Fig. 1.** Schematic illustration of balloon angioplasty. (A–C) DEB and (D–F) MNDLB applications to the atherosclerotic stenosis artery. Drug delivery efficiency was enhanced in MNDLB by 808 nm ring laser stimulation to detach drug-loaded MN tips in tissue.

to reported research [20]. In brief, PVA was added in DI water to make a 10% (w/v) solution, which was then heated to 96 °C and stirred for 2 h until the PVA powder was fully dissolved. PVA solution was poured into the molds and solidified at room temperature. The solidified PVA samples were crosslinked by freeze-thaw cycles to adjust the mechanical properties. The freeze-thaw cycle consisted of two steps: a freezing step for 12 h at –20 °C, and a thawing step for 12 h at 20 °C. The more freeze-thaw cycles, the higher elastic moduli by hydrogen bonds, thus mimicking various vessels from normal one to calcified. The tensile properties of vascular phantoms were tested by the electronic universal testing machine (WDW-30, Hualong Test).

## 2.6. Mechanical properties of MNs patch

The mechanical behavior of MNs patch was analyzed by microelectronic universal testing machine (Force Gauge, Mark-10). For the testing, MNs patch was lied on the worktable at the bottom of the testing machine. Once the MNs patch and the sensor were aligned vertically, the sensor moved down as 600 μm/min. The instantaneous stress-displacement curves were recorded.

## 2.7. Photothermal separability

In order to evaluate the photothermal separability of MNs, a ring-laser fiber 200 μm in diameter (Shanghai Youfutong Medical Equipment Co., Ltd, Fig. S2) was inserted along the catheter inner shaft and connected to the 808 nm NIR exciter (AC, HI-Tech Optoelectronics Co., Ltd.). The optical fiber retractor (Shanghai Youfutong Medical Equipment Co., Ltd.) controlled the withdrawal speed of the optical fiber. MNDLB was fixed on a vertical worktable of the testing machine. The top disc moved down at a speed of 600 μm/min, and the lateral shear stresses before and after photothermal stimulation were recorded.

## 2.8. Tissue insertion of MNs patch in vitro

The cross-shaped vascular phantom was fixed to the fixture in a mild pretension state, and the marked center was the test area as stress distributed uniformly in this area. The surface of the test area was wetted with 1% (w/v, in DI water) RhB for 1 min before MNs patch inserted down at a speed of 300 μm/min, and the stress-displacement curves were obtained. After that, residual RhB on the surface was wiped off with cotton swabs, and the puncture depth was detected by confocal microscope (LSM800, Carl Zeiss AG).

## 2.9. Temperature supervision and MNs transfer efficiency examination

MNDLB (2.5 mm × 20 mm) was inflated in a hollow cylindrical vascular phantom of 2 mm inner diameter, then the fiber was withdrawn at a constant speed and emitted 808 nm near-infrared (NIR) simultaneously in the inner shaft of the balloon catheter. Temperatures of the balloon under different laser powers and retraction speeds were recorded by infrared thermal imager (E60, FLIR). After that, the end of the balloon catheter was gently pulled by hand to break off the MN tips in the vascular phantom. Then the balloon was pulled out of the phantom after deflation, and the MN tips transferred into vascular phantom were calculated.

## 2.10. PTX release from MNs patch in vitro

To evaluate the in vitro release of PTX from MNs patches and predict the release of PTX *in vivo*, phosphate-buffered saline (PBS) with 0.02% (w/v) Tween-80 and 25% (v/v) ethanol was utilized as the release medium. MNs patch was placed in 10 mL release solution and incubated in a water bath shaker at 37 °C and 80 rpm. 1 mL release medium was collected every 5 days and replaced with the same amount of fresh medium. The collected samples were stored at 4 °C to quantify the PTX

concentration later by high performance liquid chromatography-mass spectrometer (HPLC-MS).

## 2.11. In vitro particulates loss

An extracorporeal circulation system was assembled according to previous literature [21] to obtain particulates shed from MNDLB and the control DEB. Standard vascular angioplasty were imitated: balloon catheter was inserted through a 7 F sheath and tracked 200 mm through the tubing to the vascular phantom. The flow of PBS was controlled at 150 mL/min by electric pump. When the balloon was inflated using a pressure of 8 atm (atm), the ring laser in the inner shaft was heated by 1.5 W 808 nm NIR immediately and retraced as 0.5 mm/s from balloon top to the end. After that, the fiber and the deflated balloon were pulled out of the phantom, and an additional 60 s PBS flow helped to clean up particles in the tubing. The 7 F sheath was also washed with another 40 mL PBS. All particulates were collected by a 10-μm pore size filter paper fitted on the filtration holder and imaged using the microscope (CX33, Olympus, Japan). The total particulates (diameter >100 μm), larger particulates (diameter >300 μm), and average size of the particulates was calculated using ImageJ software. Balloons and vascular phantoms were collected and frozen at –80 °C to quantify the PTX concentration later by HPLC-MS.

## 2.12. Inhibition of PTX on vascular smooth muscle cells (VSMCs)

VSMCs (A7r5, ATCC) were seeded in a 96-well plate at  $5 \times 10^3$  cells/well and cultured with Dulbecco's Modified Eagle Medium (DMEM) high sugar medium (BioInd, Israel) containing 10% fetal bovine serum (FBS, BioInd, Israel) at 37 °C under 5% CO<sub>2</sub> atmosphere for 24 h. PTX was added to each group with a graded series of concentrations (0, 0.0001, 0.001, 0.01, 0.1, 1 and 10 μM). After 24, 48 and 72 h of co-culture, the medium was changed to the medium containing 10% cell counting kit-8 (CCK-8) and cultured for 2 h. The optical density (OD) was determined using a microplate reader of VICTOR Nivo 3S (PerkinElmer, UK) at a wavelength of 450 nm. The cell viability (%) was calculated as follows:

$$\text{Cell viability (\%)} = (OD_a - OD_b) / (OD_c - OD_b) \times 100\%$$

where ODA represents the OD value of cells with different concentrations of PTX, ODb represents the OD value of the blank group, and ODC represents the OD value of cells without PTX.

## 2.13. Preparation of MNs extract

After 30 min of UV exposure, the MN-PTX patch was added to DMEM medium or 0.9% NaCl solution (containing equivalent PTX to 1 μM PTX solution) and shaken 80 rpm at 37 °C for 72 h. The extraction solution was used for subsequent experiments.

## 2.14. Migration assay

VSMCs were cultured in 6-well plates until more than 90% confluent, and scratch wounds were generated using a sterile pipette tip (200 μL). Cells were divided into four groups: control group with serum-free medium, PTX group with serum-free medium containing 1 μM PTX, MN group and MN-PTX group using its extraction solution respectively as mentioned above. After 0, 12 and 24 h, images of three different fields of each scratch were acquired, and the percentage of wound closure was quantified by measuring the residual distance of the scratch using ImageJ software.

## 2.15. Live/dead cell staining assay

VSMCs were seeded in a 96-well plate at the density of  $2 \times 10^3$  cells/

well, and divided into four groups as above with 10% FBS. After incubation for 24 h, the medium was displaced with 1 mL of PBS containing 5  $\mu$ L Calcein-AM/PI, and cells were imaged under inverted fluorescence microscopy after another 20 min of incubation.

### 2.16. Inhibition of MNs on human umbilical vein endothelial cells (HUVECs)

HUVECs (self-supply by our lab) were seeded in a 96-well plate at  $5 \times 10^3$  cells/well and cultured with Dulbecco's Modified Eagle Medium (DMEM) high sugar medium (BioInd, Israel) containing 10% fetal bovine serum (FBS, BioInd, Israel) at 37 °C under 5% CO<sub>2</sub> atmosphere for 24 h. Cells were divided into four groups as section 2.15, and cell viability were calculated as section 2.12.

### 2.17. Hemolysis assay

Red blood cells (RBCs) were isolated from Sprague Dawley rats. 100  $\mu$ L RBCs was added to 1.1 mL 0.9% NaCl solution as negative control and to 1.1 mL DI water as positive control. In the experimental groups, 100  $\mu$ L RBCs was mixed with 1.1 mL MN or MN-PTX extraction solution (0.9% NaCl solution as extraction medium) or 1  $\mu$ M PTX (0.9% NaCl solution as solvent). After incubation at 37 °C for 2 h, the absorbance of the supernatant at 540 nm was detected. The hemolysis rate of each group was calculated as follows:

$$\text{Hemolysis rate (\%)} = (OD_0 - OD_1) / (OD_2 - OD_1) \times 100\%$$

where OD<sub>0</sub> represents the OD value of the experimental groups, OD<sub>1</sub> the negative control group, and OD<sub>2</sub> the positive control group.

### 2.18. Animal study

In this study, 48 male New Zealand white rabbits (3.0–3.5 kg) were used for: 1) drug metabolism study, 2) security test, and 3) therapeutic efficacy research. All experiments were conducted in accordance with the guidelines and approved by the ethics committee of Nanchang University (Nanchang, China, SYXK 2018–0006). To develop the atherosclerotic model, the right carotid artery of each rabbit was frosted with 0.5 mL liquid nitrogen 3 times for total 2 min, and rabbits were fed with 1% cholesterol for 4 weeks [22].

Balloon angioplasty was performed 1 month later, when stenosis rate was confirmed to be 60–70% by ultrasonography. When the balloon catheter inserted into the right common carotid artery, the pressure pump inflated the balloon with 1:1 balloon-artery ratio. In microneedles balloon (MNB) and MNDLB groups, a ring-laser fiber was then introduced into the catheter's inner shaft, which was withdrawn as 0.5 mm/s and emitted 808 nm near-infrared (NIR) simultaneously to heat and melt the phase-change material LA in the MN tips. In the control group, the carotid artery was incised and sutured without balloon dilatation. Following the operation, balloons were cut off, sealed in a plastic container and frozen at –80 °C for later drug testing. The rabbits were on a normal diet. Blood biochemistry, ultrasonography and computerized tomography angiography (CTA) were performed at the set time points.

### 2.19. CTA

CTA was performed at pre-determined time points (0, 30, 90, 180 days). Contrast agent Onepike (diluted to 200 mg/mL, 8 mL) was injected at 0.5 mL/s by high pressure syringe (Ulrich, Germany) through a 24 G venous indwelling needle inserted in the left auricular vein. The scanning parameters of 128-layer spiral CT (Light Speed, GE, USA) were 120 kV, 100 mAs, 5 mm slice thickness, 2 s delay time and 30 s scanning time. The carotid artery was measured by the vascular evaluation software (syngovia, Siemens) on the CT workstation.

### 2.20. Ultrasonography

Carotid ultrasonography was performed preoperatively and post-operatively (0, 1, 30, 90 and 180 days). Anesthesia was induced with 3–5% isoflurane inhalation and maintained with a mask. The stenosis of the common carotid artery was detected by an ultrasonic diagnostic instrument (VINNO 6, Feinuo Technology Co., Ltd., China) along the direction of the carotid artery. Stenosis rate = (maximum proximal internal diameter – narrowest internal diameter)/maximum proximal internal diameter.

### 2.21. Histological analysis

The harvested vessels were rinsed with saline, fixed in 10% neutral formalin solution, and embedded in a paraffin block. The paraffinized samples were sectioned to a thickness of 4  $\mu$ m and stained with hematoxylin and eosin (H&E, Merck, Germany) for further histopathological and morphological analysis. The pathological sections were used to observe the intimal hyperplasia under 40  $\times$  and 100  $\times$  light microscope. ImageJ was used to analyze the internal elastic lamina area (IELA) and lumen area (LA). Neointimal area (NA) = IELA – LA, and the percentage of area stenosis (% AS) = NA/IELA  $\times$  100%.

### 2.22. SEM

The puncture injury caused by MNs balloon and endothelialization of blood vessel wall were observed by SEM. The arteries were fixed with glutaraldehyde and dissected along the axial direction. After gradient ethanol dehydration, critical point drying and coating, the samples were observed by SEM.

### 2.23. Degradation of needle tip in vivo

Vascular specimens were fixed with formalin and scanned by Sky-scan1278 MicroCT with a thin layer of 0.1 mm. The 3D image of intravascular needle tip was reconstructed by Mimics Medical 21.0 software (Materialise, Belgium).

### 2.24. PTX concentration

PTX concentration was measured by HPLC-MS. The frozen vascular phantoms, vessels, balloons and plasma were thawed firstly, and ethyl acetate/dichloromethane/acetonitrile (w/w/w = 4/1/1) was prepared as extraction reagent, with docetaxel/methanol as the internal standard solution (800  $\mu$ g/mL for vessels and balloons, and 0.1  $\mu$ g/mL for plasma). Firstly, blood vessels (or balloons)/extraction reagent/internal standard solution (1 g/5 mL/1 mL), or plasma/extraction reagent/internal standard solution (0.2 mL/4 mL/0.1 mL) was sonicated for 30 min, vortex mixed for 1 min, and centrifuged at 5000 rpm for 20 min, then the supernatant was taken and evaporated with a nitrogen evaporator. The residue was re-dissolved with mobile phase, and then 2  $\mu$ L was taken for LC-MS analysis. Agilent 1260 liquid chromatography-G6430 triple tandem quadrupole liquid chromatograph (Agilent Technologies, USA) was used, and its working parameters were set as follows: electrospray ion source with a Vcap 4000 V, drying gas temperature 350 °C, atomization gas pressure 30 psi, and drying gas flow 10 L/min. The collision energies of both PTX and docetaxel were 22 eV, and the cleavage voltages were 250 eV and 210 eV, respectively. Agilent SB-C18 column (3.5  $\mu$ m, 2.1 mm  $\times$  150 mm) worked with methanol/0.1% formic acid water (95/5, v/v) as mobile phase. The flow rate of mobile phase was 0.3 mL/min, and the column temperature was set as 30 °C.

### 2.25. Statistical analysis

In order to avoid batch-to-batch errors, the samples were measured centrally, and the blind method was applied to the surveyors. All data

were expressed as means ± staining deviation (s.d.). Statistical analyses were performed using GraphPad Prism (GraphPad Software, Inc., San Diego, CA) by the one-way analysis of variance (ANOVA) and *t*-test. The threshold of statistical significance was  $p < 0.05$ .

### 3. Results and discussion

#### 3.1. Design and fabrication of rapidly separable MNs patches

When designing MNs patches, classical antiproliferative drug PTX was chosen. PTX prevents the depolymerization of tubulin dimer in VSMCs, thus inhibiting cell mitosis and triggering apoptosis [23]. PCL is an interesting material for bone tissue engineering scaffolds and other applications due to its excellent mechanical property, good biocompatibility and slow degradation that as long as more than one year *in vivo* [24,25]. Due to the faster degradation rate of PLGA [26,27], it was added to PCL to formulate mixtures as MN materials which were expected to release drug from weeks to months. Biocompatible light-cured resin was utilized to firmly connect the tip of the needle to the balloon surface. In order to break off the tip rapidly, thermosensitive LA, melting

point 44 °C, was selected so as to minimize thermal damage to the human body when it was applied locally and temporarily [28–30].

Fabrication of MNDLB was shown in Fig. 2A. After the first casting, PTX loading was about 0.56 or 0.57  $\mu\text{g}/\text{mm}^2$  for the balloons. The second casting gave the balloons PTX loading 1.12 and 1.14  $\mu\text{g}/\text{mm}^2$ , respectively (Tab. 1), lower than 2  $\mu\text{g}/\text{mm}^2$  of the control DEB. It has been reported that appropriate reduction in DEB drug loading could achieve the similar therapeutic effect, which could even reduce some drug loss and drug-related complications [31,32]. Considering that the drug loss of DEB would be higher than MNDLB, this lower drug loading was chosen for MNDLB. For better visualization, white PTX was replaced by melanin, and thermosensitive tip-separable melanin-loaded balloons were fabricated (Fig. 2B–D). Each needle possessed a conical shape, with base diameter of 300  $\mu\text{m}$ , height of 500  $\mu\text{m}$ , tip diameter of 10  $\mu\text{m}$ , and interval between MN tips of 900  $\mu\text{m}$ . The height of the drug-loaded tip was measured to be  $276.54 \pm 12.41 \mu\text{m}$  (Fig. 2E), and the surface structures of the tip and base before (I–II) and after (III–IV) photothermal stimulation kept almost the same. The test of melting point of LA and its mixture with PCL/PLGA by DSC showed that the melting point of LA decreased a bit from 45.30 °C to 44.40 °C when mixed with

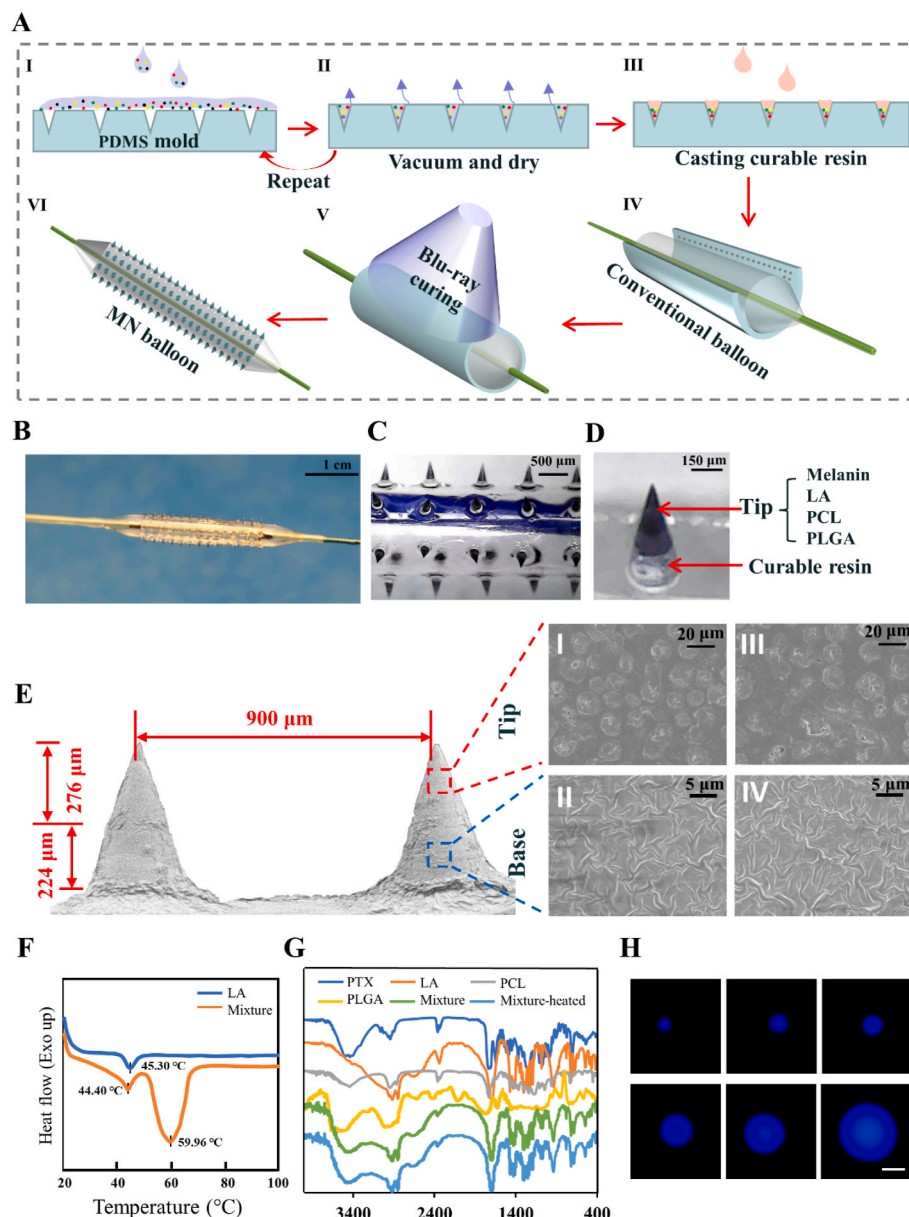


**Fig. 2.** Fabrication schematic and characterizations of MNDLB. (A) Conformal transfer molding process consisting of: (I–II) drug-loaded tips fabrication; (III) MN bases fabrication; (IV) alignment of flexible planar PDMS mold; (V) curing process and (VI) completed MNDLB. (B) Dilated MNDLB. (C–D) Two-section MNs on MNDLB. For better visualization, white PTX was replaced by alcohol soluble melanin. (E) The surface structures of the tip and base before (I–II) and after (III–IV) photothermal stimulation kept almost the same. (F) DSC of LA and its mixture with PCL/PLGA. The melting point of LA decreased a bit from 45.30 °C to 44.40 °C when mixed with PCL/PLGA. (G) The FTIR of the tip mixture and its components. No abnormal absorption peak detected, and the curves before and after photothermal intervention unchanged. (H) The tip sections with AMC-LA. The fluorescence was uniformly distributed. Scale bar = 100  $\mu\text{m}$ .

PCL/PLGA, and the endothermic peak of PCL was also found at 59.96 °C (Fig. 2F). The FTIR of the needle tip and its components were shown in Fig. 2G. Each component was mixed together physically, and no abnormal absorption peak was detected. Also, the curves of the needle tip before and after the photothermal stimulation did not remarkably change. Besides, the needle section showed that AMC-LA was uniformly distributed with no difference in fluorescence intensity (Fig. 2H). To sum up, the characterizations of MNs using SEM, FTIR, and fluorescence imaging showed that the drug-loaded tips were homogenous and the LA and PTX was uniformly dispersed in the mixture.

### 3.2. Mechanical performance and penetration of MN

In order to reach the lesion through the blood vessels, MNs array must be firmly adhered to the balloon. Besides, MN itself should be tough enough to avoid fragmentation and debris under pressure. Furthermore, the MN should have sufficient mechanical strength to pierce into the fibrotic or even calcified vascular tissue. We detected that the MN strength during compression increased with increasing PCL ratio (Fig. 3A–B), but an appropriate amount of PLGA was needed to facilitate early drug release. Finally, PCL/PLGA = 1/1 (w/w) was chosen for MNDLB, in which case the MN could withstand  $\geq 0.2$  N/needle at the pressed distance of 300  $\mu\text{m}$ . This mechanical strength was expected to be sufficient referring to its applications in skin tissue [33–35].

After photothermal excitation, the tip was easily shed under the shear force of a 3-0 surgical suture (Video S1). In contrast, this shear force would not break off the MN without photothermal excitation (Video S2). Fig. 3C–D show the stress-strain curve of MNs under shear force without photothermal excitation. When the force disappeared, the bent MN could rebound quickly without break. The power of 808 nm NIR and the retraction speed of ring laser fiber were related to the shear force for tip detachment (Fig. 3E). For example, when the optical fiber was pulled back fast, the LA at the interface between tips and bases melted incompletely, resulting in higher shear force. When optical fiber was retracted as 0.5 mm/s, the lateral shear forces under 1 W and 1.5 W were  $0.063 \pm 0.003$  N and  $0.051 \pm 0.004$  N, respectively, with no statistical difference, while 0.5 W NIR required significantly higher shear force. The above results indicated that both 1 W and 1.5 W were sufficient to completely melt the LA between the tips and bases, while under 0.5 W, LA was only partially melted.

Supplementary video related to this article can be found at <https://doi.org/10.1016/j.bioactmat.2022.11.015>

In order to verify the puncture ability in this case, vascular phantoms with elastic modulus ranging from  $9.80 \pm 3.13$  to  $275.80 \pm 11.76$  kPa (Fig. S3) were prepared to simulate normal to fibrotic to calcified vascular tissue. The stress-strain curves were obtained (Fig. 3F–G), and there were three phases in this process: I) the initial phase, when the needle was just in contact with the vessel and there was no interaction force, corresponding to the origin of the curve; II) the moment when needle tip just inserted into the blood vessel, with a turning peak in the curve (marking the instant resistance reduction); III) the phase that needle tip penetrated in the blood vessel until it reached the endpoint (the maximum pressure on each MN was expected to be 0.04 N and maximum displacement 1 mm, according to the working pressure (8 atm) of the non-compliant balloon). Therefore, the depth of the tip in the wall was the distance of phase II to III. It was worth mentioning that for 1 freeze-thaw cycle phantom, the phantom wall could expand well as the balloon expanded, which led to the penetration depth less than 200  $\mu\text{m}$ . That meant the detached MN tip embedded in tissue partially. The penetration depth in tissue pre-wetted by RhB (Fig. 3H) for 1 min was measured by confocal fluorescence (Fig. 3I), whose results were consistent with the stress-strain curves. Then, MN puncture ability was detected in the hollow cylindrical vascular phantoms (Fig. 4A–B), with 1 W NIR and optical fiber pulled back at 0.5 mm/s 100% MN tips were embedded in the tissue, and the MN bases still adhered firmly to the balloon (Fig. 4C–D).

The balloon and catheter are made of polyethylene terephthalate (PET), whose glass transition temperature is about 70 °C [36]. The temperatures under different powers of 808 nm NIR were recorded by infrared camera when the fiber was fixed and heated for 1 min inside the balloon catheter (Fig. 4E–F). Furthermore, the local temperature of vascular phantoms gradually rose and fell when the fiber was withdrawn inside the balloon as 0.5 mm/s. The extraluminal maximum temperatures were about 43–48 °C (Fig. S4) with different NIR powers. Certainly, the intraluminal maximum temperature was a bit higher (unable to detect directly). In order to avoid the balloon damage and tissue injury caused by high temperature, NIR was set to 1 W in the later animal experiments.

SEM images showed the gradual degradation of MN tips when PCL/PLGA = 1/1 (w/w, Fig. S5A). As PLGA increased in MN, the early release and total release of drugs during the six months increased (Fig. S5B) without initial burst release. The MNs could be reformulated to adjust the release duration to address the different needs.

### 3.3. Particulates loss in extracorporeal circulation system

Drug particulates or coating fragments shed from DEB may be associated with small vessels occlusion or capillaries micro embolization. It has been documented in the literature that higher dose of PTX resulted in more debris embolization and PTX-related fibrinoid necrosis in distal areas [37,38]. A Food and Drug Administration (FDA) safety communication has presented nine mortalities related to polymer separation from intravascular devices, and pointed out that it likely represented an underestimate of the actual occurrence [39]. Standard angioplasty in assembled extracorporeal circulation system (Fig. 5A) showed that our MNDLB addressed the problem of drug loss well. As shown in Fig. 5B–C, the total number of particulates (diameter >100  $\mu\text{m}$ ) and larger particulates (diameter >300  $\mu\text{m}$ ) of MNDLB were  $1589.0 \pm 103.0$  and  $42.7 \pm 18.5$ , respectively, which were less than that of DEB group ( $5088.0 \pm 325.0$  and  $309.0 \pm 48.9$ , respectively). In addition,  $77.67 \pm 2.50\%$  of the drug was transferred to the blood vessel wall in MNDLB group, and drug loss into the blood stream was  $12.00 \pm 2.16\%$ , which were significantly more satisfactory than that of DEB group ( $37.33 \pm 4.19\%$  and  $20.33 \pm 3.40\%$ , Fig. 5D). Although the average particulate size of MNDLB was slightly larger than that of DEB ( $179.5 \pm 9.7$   $\mu\text{m}$  and  $146.5 \pm 7.4$   $\mu\text{m}$ , respectively), the MNDLB had tiny possibility of occlusion in major distal vessels (vessels larger than 300  $\mu\text{m}$ ) during angioplasty. What's more, the maximum local temperature of the vascular phantom was about 45 °C when the 808 nm ring laser was 1 W and retracted at 0.5 mm/s (Fig. S6).

### 3.4. MNDLB inhibited the proliferation and migration of cells in vitro

Balloon dilation to the stenotic artery by air pressure can also cause endotheliocyte shedding, fiber breakage and plaque rupture, which can induce inflammatory responses as well as the proliferation and migration of VSMCs, eventually resulting in restenosis [40]. The evolution of restenosis can differ widely, depending on the target region, balloon pressure, dilation time and so on [41,42]. The proliferation and migration of VSMCs are important pathological factors of restenosis. Herein, whether the PTX released from MNs could inhibit the activity of VSMCs was investigated. Firstly, it was confirmed that PTX of  $1 \times 10^{-2}$   $\mu\text{M}$  and above could inhibit the proliferation of VSMCs by CCK-8 assay (Fig. S7). Since the concentration of PTX in the extraction solution might be very limited, 1  $\mu\text{M}$  PTX and extraction solution with the same amount of PTX in MNs were chosen for cell experiments.

Live/dead cell staining at 24 and 72 h showed a significant increase in cell density in the control and MN groups, while in the MN-PTX group, especially the PTX group, VSMCs density was lower than control group, and cell death was also significantly increased (Fig. S8). Migration assay (Fig. S9) showed that VSMCs in control group presented obviously rapid scratch healing. MN-PTX group, especially the PTX group, had a

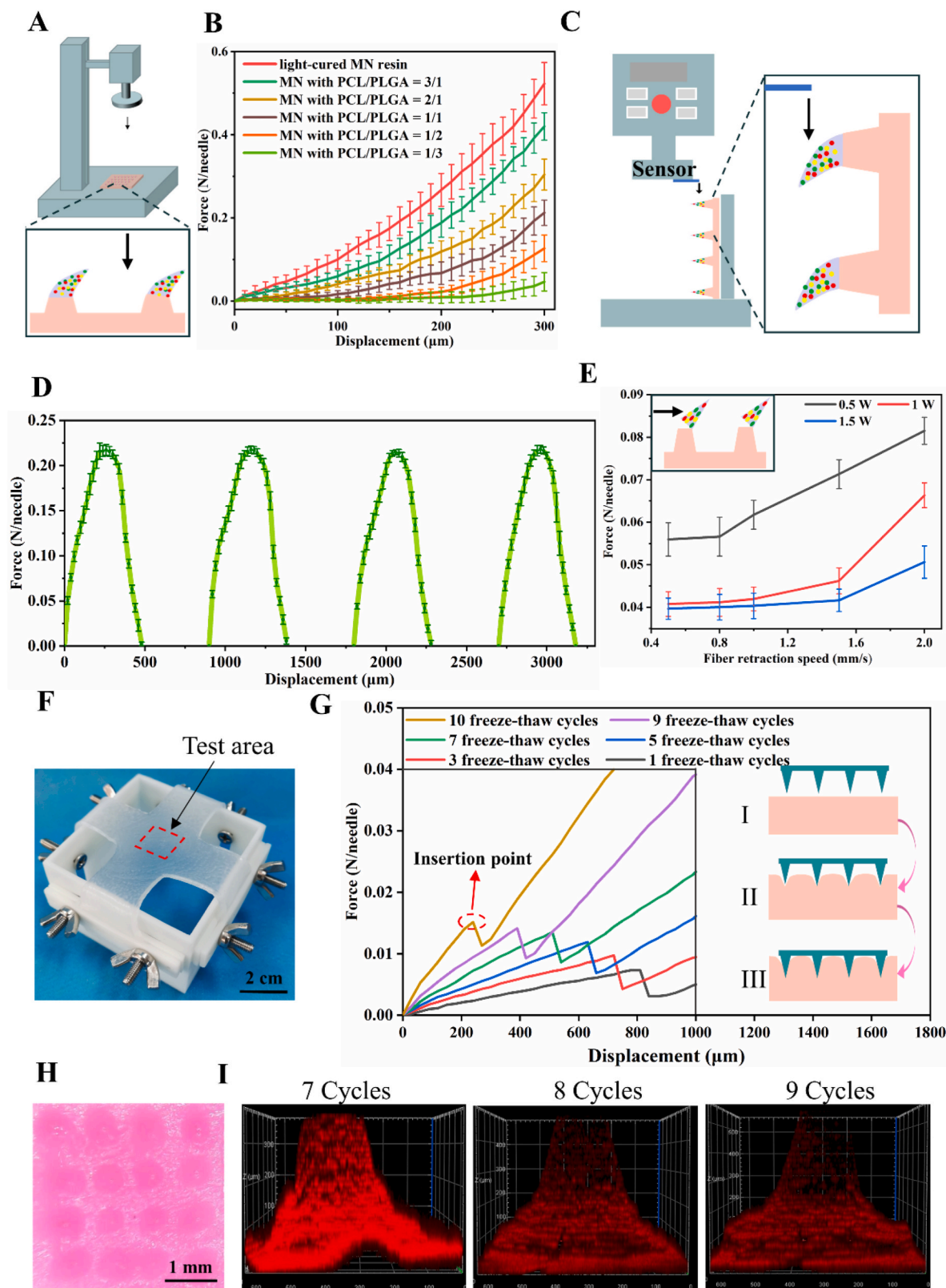


**Fig. 3.** Mechanical performance and penetration of MN. (A, C) Schematic diagrams of the experimental setups. Stress-strain curves of MN under vertical compression force (B) and horizontal shear force (D). (E) The shear forces for tip detachment at different powers of 808 nm NIR and retraction speeds of ring laser fiber. (F) Vascular phantom fixed to the fixture by the fixing holes and bars. The marked center was the test area. (G) Stress-strain curves of vascular phantoms with different hardness. Schematic diagram showed the three phases in this process: I) the initial phase; II) the moment when MN tips just inserted into the blood vessel; III) the phase that the needle tip penetrated into the blood vessel until it reached the endpoint of force 0.04 N or displacement 1 mm. The penetration depth in tissue pre-wetted by RhB (H) for 1 min was measured by confocal fluorescence (I). Data are means  $\pm$  s.d., n = 3.

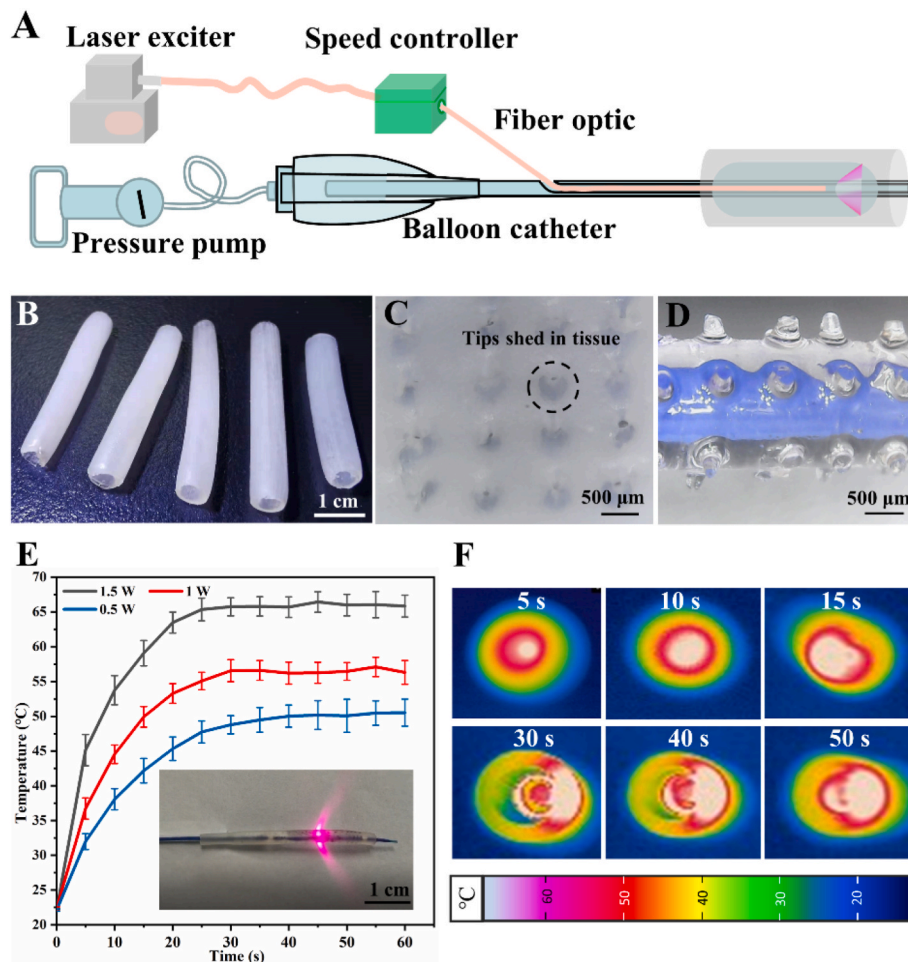


**Fig. 4.** Photothermal separability test of MNDLB. (A) Schematic of MNDLB angioplasty in vitro. (B) Hollow cylindrical vascular phantoms. (C) Drug-loaded tips embedded in the phantom. (D) MNDLB after MN tips detachment. (E) The temperature changes when the fiber was fixed and heated for 1 min inside under different powers of 808 nm NIR. (F) Infrared camera recorded the temperatures under 1 W of 808 nm NIR. Data are means  $\pm$  s.d. ( $n = 3$ ).

significantly wider scratch width than the control group. We concluded that PTX released by MNs was sufficient to inhibit VSMCs proliferation and migration. In the hemolysis test (Fig. S10), no obvious hemolysis reaction was observed in each experimental group, reflecting the safety of MN-PTX and MN in the circulatory system. Noteworthy, PTX and MN-PTX from MNs could also inhibit the proliferation of HUVECs (Fig. S11), which might be disadvantageous to vascular endothelialization after MNs insertion.

### 3.5. Safety and efficacy of MNDLB

Safety is the fundamental issue in clinical application. In addition to the MN-based puncture injuries, there might be complications of tips dislodgement or vessel rupture when MNs pierced into the tissue too shallowly or too deeply. Besides, the long-acting release of PTX may have a sustained inhibitory effect on endothelial cell healing and induce thrombosis [43]. Furthermore, needle tips were scattered in tissues, leading to varied drug concentrations in tissues, which might end in regionally inconsistent therapeutic effect. For these reasons, the safety of MNDLB should be monitored cautiously. The successful construction of atherosclerotic animal model (Fig. S12) by liquid nitrogen frostbite was confirmed by ultrasonography. The four experimental groups used in this comparative study were defined as control group (positive control), DEB group, MNB group and MNDLB group. After balloon dilation in the stenotic carotid artery (Fig. S13), the ring-laser fiber was introduced into the inner shaft of the balloon catheter. The maximum local temperature

of the vessel was about 44 °C when the 808 nm ring laser was 1 W and retracted at 0.5 mm/s (Fig. S14). Certainly, the intraluminal maximum temperature was a bit higher, but it couldn't be measured directly. All of our animals survived without negative clinical signs until the set time points (Fig. 6A). Blood routine and blood biochemistry were all in the normal range (Fig. S15), and no pathological changes were seen in the crucial organs (Fig. S16). Ultrasonography was performed in all rabbits on day 1 after balloon intervention, and no procedure-related complications such as dissection, thrombosis or vessel rupture were detected. Besides, the degree of stenosis improved significantly in all three angioplasty groups (from 61 to 69% preoperatively to 13–18% post-operatively), with no statistical difference among the groups (Fig. 6B).

As shown in Fig. S17A, MN marks were found in the lumen of the treated vessels of 200–400  $\mu$ m in depth. Despite the variation of MN incision depths, MN could penetrate vascular tissue to a depth sufficient to overcome the endothelium (<10  $\mu$ m) without breaking the adventitia layer. MN marks were also seen by SEM 1 day after intervention, but on day 28, tips-embedded vascular were basically endothelialized (Fig. S17B–C), indicating that MN insertion was safe in terms of endothelialization.

The progress of intimal hyperplasia was monitored with ultrasonography, CTA and H&E section after angioplasty (Fig. S18). Undesired intimal proliferation evolved in the three angioplasty groups, especially in the MNB group (Fig. 6B–C, 7A) indicating the deceleration of intimal hyperplasia by DEB and MNDLB. At the 6th month, the progress of intimal hyperplasia in MNDLB group was significantly slower than

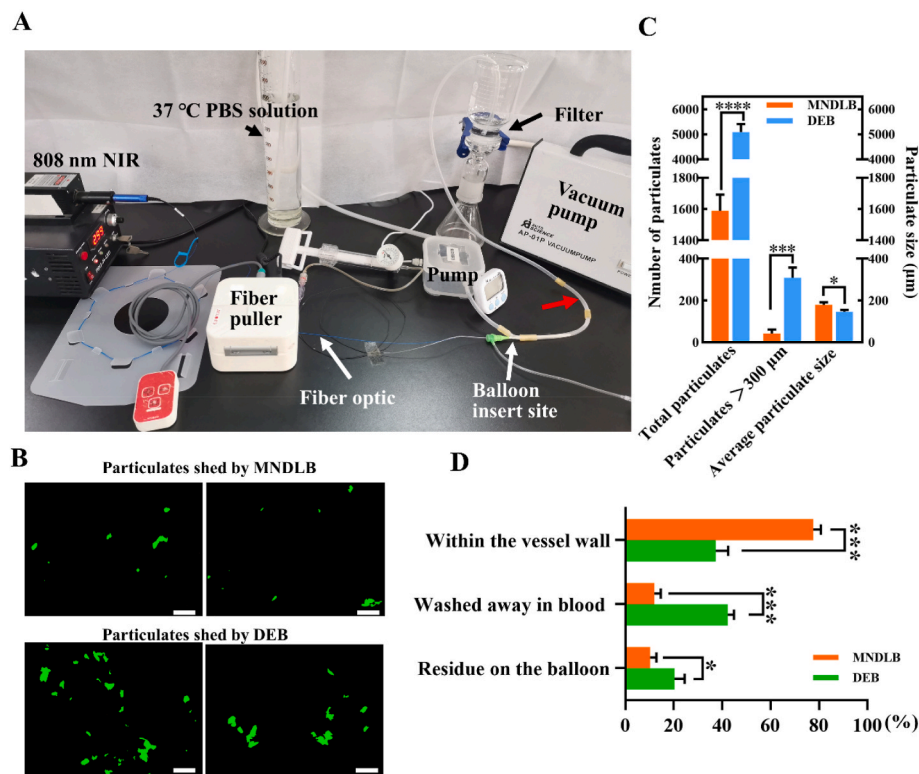


**Fig. 5.** *In vitro* particulates loss. (A) Standard angioplasty in assembled extracorporeal circulation system to obtain particulates shed from MNDLB and the control DEB. The red arrow points the balloon inflation site in vascular phantom. (B) Particulates collected on filter paper (particulates converted to green in black background using ImageJ software). Scale bar = 300 μm. (C) Quantitative analysis of particulate number (diameter >100 μm or > 300 μm) and average particulate size. (D) Drug distribution. About 80% of the drug was transferred to the vascular tissue in MNDLB group, much higher than that in the DEB group. Data are means ± s.d., n = 3. \**p* < 0.05, \*\**p* < 0.001, \*\*\**p* < 0.0001.

others (Figs. 6D and 7B). We inferred that persistent PTX release by the degradation of polymers could inhibit intimal hyperplasia for a longer time.

### 3.6. Drug metabolism

Drug content in vessel wall was  $89.12 \pm 9.74\%$  (Fig. S19), and drug remained on the balloon was  $7.33 \pm 3.62\%$ , suggesting  $3.65 \pm 2.18\%$  of the drug was lost. Compared with the results of extracorporeal circulation system *in vitro*, the increase of drug transfer and decrease of drug loss probably owed to more drug lost as balloon passed through the sheath and pipeline in the standard surgical procedure. DLB, whose drug paclitaxel and carriers (benzoate and polyethylene glycol) were repeatedly dripped onto the surface until the drug concentration reached  $2 \mu\text{g}/\text{mm}^2$ , was inferior to MNDLB in drug delivery efficiency and drug loss rate ( $45.21 \pm 10.35\%$  and  $37.96 \pm 7.35\%$ , respectively). The plasma drug concentrations were too low to be detected 72 h later in both groups (Fig. 7C). Drug content in vessel wall and cumulative drug release were shown in Fig. 7D. In MNDLB group, PTX in MN tips was released gradually, and drug concentration in the lesion after 180 days was  $69.99 \pm 21.46 \mu\text{g}/\text{g}$  (cumulative release  $84.38 \pm 3.27\%$ ). In DEB group, drug metabolism was more rapid, and drug concentration was  $0.30 \pm 0.16 \mu\text{g}/\text{g}$  on day 30 with cumulative release nearly 100%. Although it is unknown what minimal PTX concentration in the tissues is required to inhibit intimal hyperplasia, the PTX measured in the tissues of MNDLB were within the concentration range to inhibit VSMCs proliferation [44,45]. Therefore, MNDLB retained a therapeutic level of drug up to 180 days.

The three-dimensional reconstructions of the tips in the tissue by microCT were shown in Fig. 7E. At 1st month, the implanted tips began to degrade but still maintained their original shape. At the 3rd month, the tips were significantly degraded. After 6 months, the tips were degraded to smaller particles but still incompletely degraded. In addition to the comparison with drug-coated balloon in this paper, we also compared the drug delivery efficiency and stenosis-inhibiting effect of

MNDLB with the literature, as shown in Tab. 2 [46–52].

### 3.7. Study limitations and future work

Even though the penetration ability of MNDLB was demonstrated *via* vascular phantoms and AS animal model, it does not represent all the actual situations. For example, in the case of long circular calcification of diabetic AS, the penetrating ability of MNDLB can be quite different and further experimental studies are needed. In addition, the MNs on the balloon's surface would increase the diameter of the catheter and hinder its crossability in the lumen. While the crossability was not measured since *in situ* incision was used instead of femoral artery puncture in this simplified operation [20]. What is more, we only observed the results for 6 months postoperatively in animal, at which time, neither the drug had been released completely nor the polymer had been degraded thoroughly. Whether late onset restenosis caused by polymers eliciting foreign body response needs further investigation [53,54].

## 4. Conclusion

In this study, we have developed a thermosensitive tip-separable MNDLB, with sufficient mechanical strength to penetrate the blood vessel and rapid MN tips detachment ability under NIR stimulation. Compared with the standard DEB, MNDLB provided optimal drug transfer to the target tissue and exerted long-acting anti-proliferation. Although future translation and application of MNDLB will require a number of additional considerations, further development of this balloon-based drug delivery technology may bring new hope for atherosclerosis treatment, as well as for other diseases requiring intraluminal targeted drug delivery, such as esophagostenosis, bronchiostenosis and ureterostenosis.

### Ethics approval

All animal experiments were conducted in accordance with the

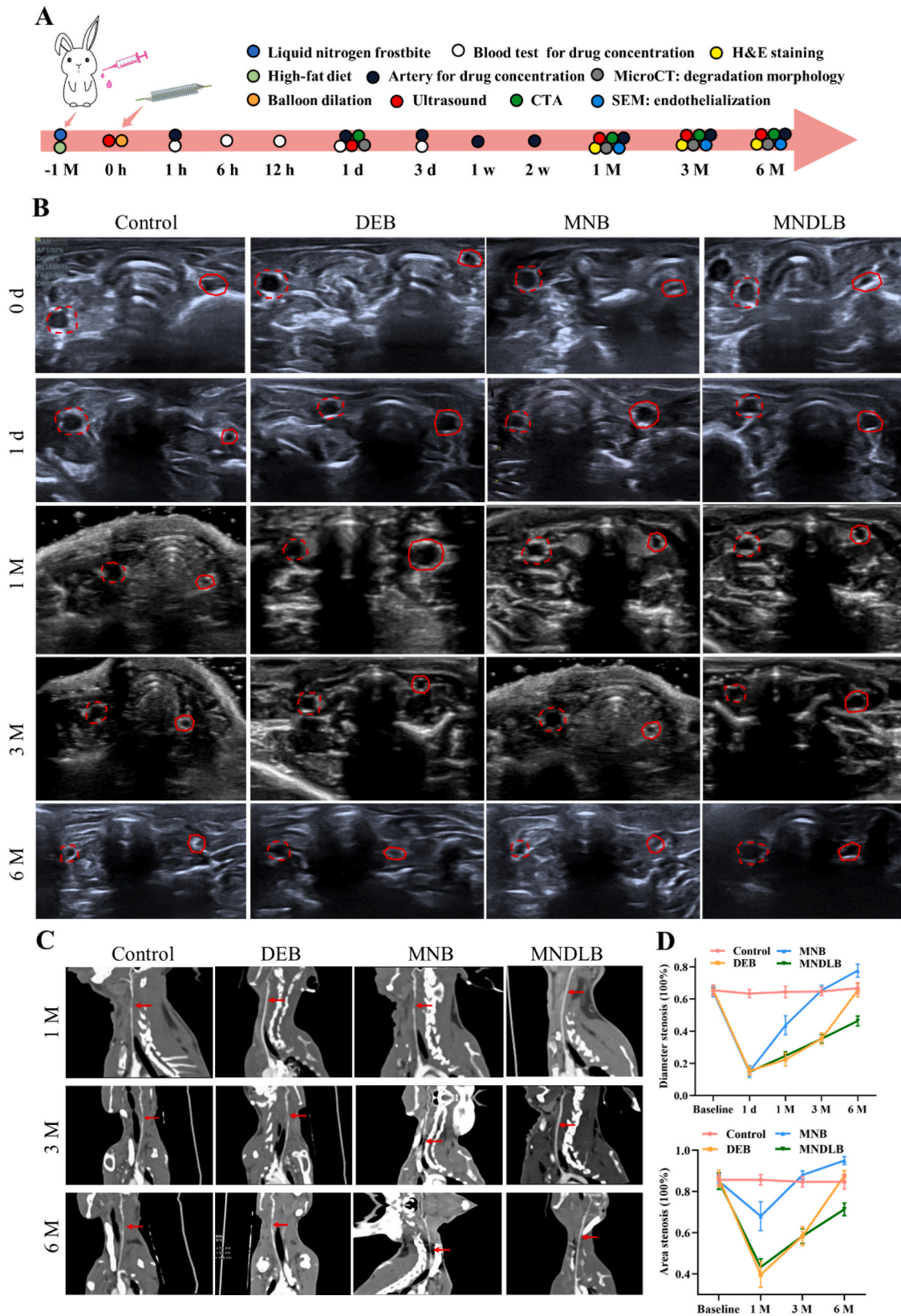


**Fig. 6.** Therapeutic efficacy of MNDLB to stenotic carotid arteries. (A) Experiments performed at indicated time points (d = day, w = week, M = month). (B–C) Evaluation of arterial stenosis rate by ultrasonography and CTA in each group at 0 d, 1 d, 1 M, 3 M and 6 M after operation (the red solid lines mark the operated side, and red arrows point the narrow segment). (D) Quantitative analysis of the carotid artery stenosis rate. Diameter stenosis was monitored with ultrasonography (upper), and area stenosis with CTA (bottom). At 6 M, the arterial stenosis rate in the MNDLB group was significantly lower than other groups. Data are means  $\pm$  s.d., n = 3.

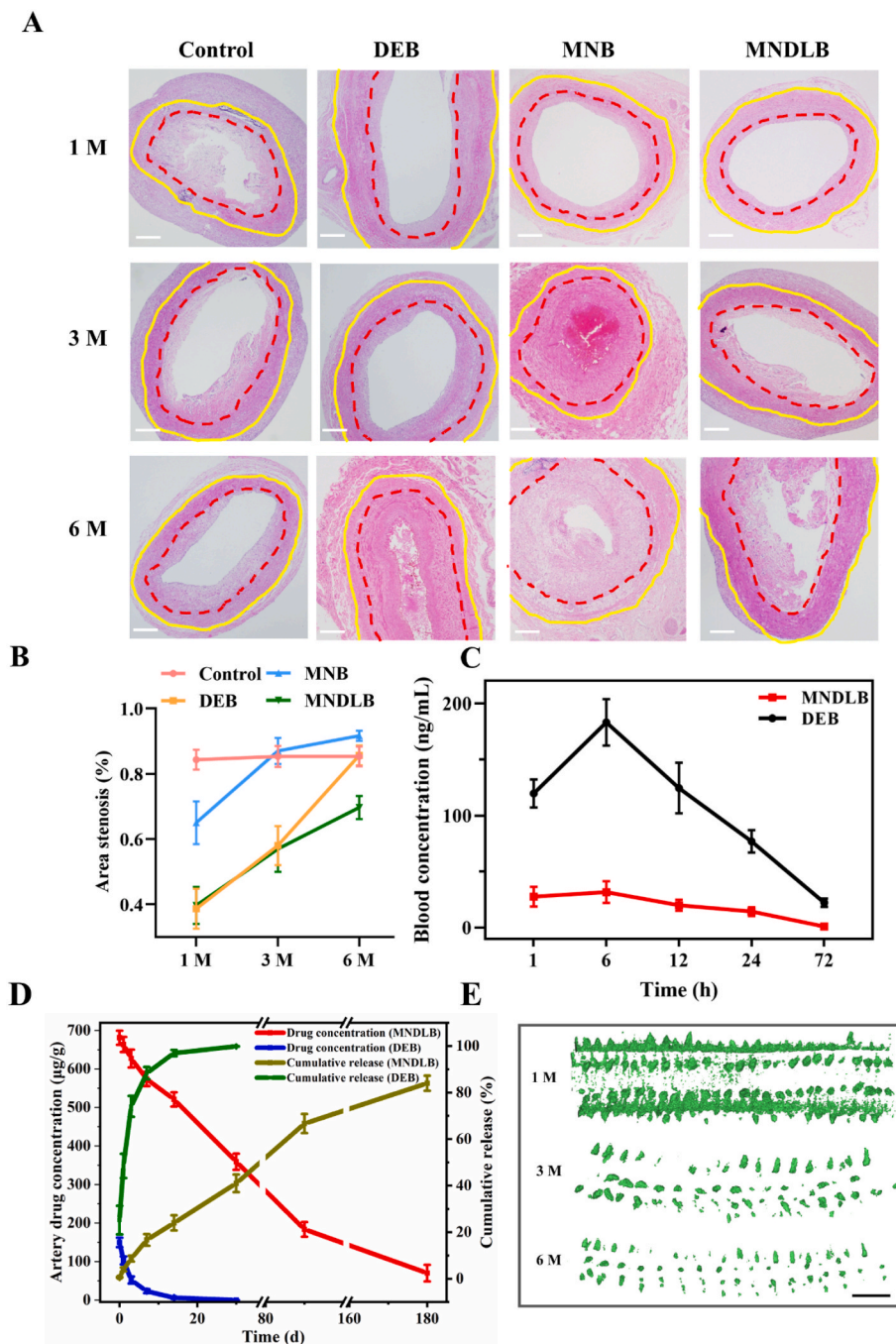


**Fig. 7.** Histological analysis and drug metabolism. (A) H&E staining of carotid artery after angioplasty. The red dotted lines mark the internal elastic lamina, and the yellow solid lines mark the external elastic lamina. Scale bar = 250  $\mu\text{m}$ . (B) Quantitative analysis of stenosis rate by H&E staining. At sixth month, the arterial stenosis rate in the MNDLB group was significantly lower than other groups. (C) Drug concentration in plasma, which was too low to be detected after 72 h. (D) Drug content in vessel wall and cumulative drug release. (E) Reconstructions of the tips in the tissue by microCT. Microneedles degraded gradually over time. Scale bar = 1 mm. Data are means  $\pm$  s.d.,  $n = 3$ .

guidelines and approved by the ethics committee of Nanchang University (Nanchang, China, SYXK 2018–0006).

#### CRediT authorship contribution statement

**Li Huang:** Conceptualization, Methodology, Validation, Formal analysis, Writing – original draft. **Huaqiang Fang:** Methodology, Validation, Formal analysis. **Teng Zhang:** Ultrasonography. **Binbin Hu:** Investigation, Resources. **Shichen Liu:** Formal analysis. **Fanzhen Lv:** Investigation, Resources. **Zhaoxia Zeng:** CTA. **Huijie Liu:** Data curation. **Weimin Zhou:** Supervision, Funding acquisition. **Xiaolei Wang:** Conceptualization, Writing – review & editing, Project administration, Funding acquisition.

#### Declaration of competing interest

The authors declare that they have no known competing financial interests or personal relationships that could have appeared to influence the work reported in this paper.

#### Acknowledgments

This work was funded by the National Natural Science Foundation of China (No. 31860263 to Xiaolei Wang; No. 82060095 to Weimin Zhou), Key Youth Project of Jiangxi Province (20202ACB216002 to Xiaolei Wang), Key Research and Development Project of Jiangxi Province (20212BBG73004 to Xiaolei Wang; 20171ACG70008 to Weimin Zhou), Natural Science Foundation of Jiangxi Province (911135755018 to Weimin Zhou).

## Appendix A. Supplementary data

Supplementary data to this article can be found online at <https://doi.org/10.1016/j.bioactmat.2022.11.015>.

## Abbreviation

|         |  |
|---------|--|
| AS      | arteriosclerosis   |
| CTA     | computerized tomography angiography                      |
| DEB     | drug-eluting balloon                                     |
| HPLC-MS | high performance liquid chromatography-mass spectrometer |
| LA      | lauric acid  |
| MN      | microneedle  |
| MNB     | microneedles balloon                                     |
| MNDLB   | tip-separable microneedles drug-loaded balloon           |
| NIR     | near-infrared  |
| PCL     | polycaprolactone   |
| PDMS    | polydimethylsiloxane                                     |
| PLGA    | polylactic-co-glycolic acid                              |
| PTX     | paclitaxel   |
| PVA     | polyvinyl alcohol  |
| RhB     | Rhodamine B  |
| VSMCs   | vascular smooth muscle cells                             |
| HUVECs  | human umbilical vein endothelial cells                   |

## References

- [1] GBD 2019 diseases and injuries collaborators, global burden of 369 diseases and injuries in 204 countries and territories, 1990–2019: a systematic analysis for the global burden of disease study 2019, *Lancet* 396 (10258) (2020) 1204–1222.
- [2] S. Barquera, A. Pedroza-Tobías, C. Medina, L. Hernández-Barrera, K. Bibbins-Domingo, R. Lozano, A.E. Moran, Global overview of the epidemiology of atherosclerotic cardiovascular disease, *Arch. Med. Res.* 46 (5) (2015) 328–338.
- [3] S. Jebari-Benslaïman, U. Galicia-García, A. Larrea-Sebal, J.R. Olaetxea, I. Alloza, K. Vandebroek, A. Benito-Vicente, C. Martín, Pathophysiology of atherosclerosis, *Int. J. Mol. Sci.* 23 (6) (2022) 3346.
- [4] J.S. Lawton, J.E. Tamis-Holland, S. Bangalore, E.R. Bates, T.M. Beckie, J. M. Bischoff, J.A. Bittl, M.G. Cohen, J.M. DiMaio, C.W. Don, S.E. Frenes, M. F. Gaudino, Z.D. Goldberger, M.C. Grant, J.B. Jaswal, P.A. Kurlansky, R. Mehran, T. S. Metkus, L.C. Nnacheta, S.V. Rao, F.W. Sellke, G. Sharma, C.M. Yong, B. A. Zwischenberger, ACC/AHA/SCAI guideline for coronary artery revascularization: executive summary: a report of the American College of Cardiology/American Heart Association Joint Committee on clinical practice guidelines, *Circulation* 145 (3) (2021) e4–e17, 2022.
- [5] C. Yerasi, B.C. Case, B.J. Forrestal, R. Torguson, W.S. Weintraub, H.M. Garcia-García, R. Waksman, Drug-coated valloon for *de novo* coronary artery disease: JACC state-of-the-art review, *J. Am. Coll. Cardiol.* 75 (9) (2020) 1061–1073.
- [6] B. Cortese, G. Di Palma, M.G. Guimaraes, D. Piraino, P.S. Orrego, D. Buccheri, F. Rivero, A. Perotto, G. Zambelli, F. Alfonso, Drug-coated balloon versus drug-eluting stent for small coronary vessel disease: PICCOLETO II randomized clinical trial, *Jacc-Cardiovasc. Inte.* 13 (24) (2020) 2840–2849.
- [7] D. Giacoppo, F. Alfonso, B. Xu, B. Claessen, T. Adriaenssens, C. Jensen, M.J. Pérez-Vizcayno, D.Y. Kang, R. Degenhardt, L. Pleva, J. Baan, J. Cuesta, D.W. Park, P. Kukla, P. Jiménez-Quevedo, M. Unverdorben, R. Gao, C.K. Naber, S.J. Park, J.P. S. Henriques, A. Kastrati, R.A. Byrne, Drug-coated balloon angioplasty versus drug-eluting stent implantation in patients with coronary stent restenosis, *J. Am. Coll. Cardiol.* 75 (21) (2020) 2664–2678.
- [8] A.R. Tzafiri, B. Muraj, F. Garcia-Polite, A.G. Salazar-Martín, P. Markham, B. Zani, A. Spognardi, M. Albaghdadi, S. Alston, E.R. Edelman, Balloon-based drug coating delivery to the artery wall is dictated by coating micro-morphology and angioplasty pressure gradients, *Biomaterials* 260 (2020), 120337.
- [9] A. Pérez de Prado, C. Pérez Martínez, F. Fernández Vázquez, Leaving absolutely nothing behind – is there any room for improvement in drug coated balloons? *Int. J. Cardiol.* 331 (2021) 71–72.
- [10] S. Kaule, I. Minrath, F. Stein, U. Kragl, W. Schmidt, K.P. Schmitz, K. Sternberg, S. Petersen, Correlating coating characteristics with the performance of drug-coated balloons – a comparative *in vitro* investigation of own established hydrogel- and ionic liquid-based coating matrices, *PLoS One* 10 (3) (2015), e0116080.
- [11] I. Kan, K. Karagiozov, S. Ito, S. Sato, Y. Murayama, Microcatheter originating debris during neuroendovascular procedures: mechanism of dislodgement and its prevention, *Am. J. Neuroradiol.* 41 (10) (2020) 1879–1881.
- [12] R.I. Mehta, R.I. Mehta, Hydrophilic polymer embolism: implications for manufacturing, regulation, and postmarket surveillance of coated intravascular medical devices, *J. Patient Saf.* 17 (8) (2021) e1069–e1079.
- [13] S. Habara, K. Kadota, T. Shimada, M. Ohya, H. Amano, Y. Izawa, S. Kubo, Y. Hyodo, S. Otsuru, D. Hasegawa, T. Tada, H. Tanaka, Y. Fuku, T. Goto, K. Mitsudo, Late restenosis after paclitaxel-coated balloon angioplasty occurs in patients with drug-eluting stent restenosis, *J. Am. Coll. Cardiol.* 66 (1) (2015) 14–22.
- [14] E. Zapata-Arriaza, F. Moniche, A. González, A. Bustamante, I. Escudero-Martínez, F.J. De la Torre Laviana, M. Prieto, F. Mancha, J. Montaner, Predictors of restenosis following carotid angioplasty and stenting, *Stroke* 47 (8) (2016) 2144–2147.
- [15] G.M. Xiong, H. Ang, J. Lin, Y.S. Lui, J.L. Phua, J.N. Chan, S. Venkatraman, N. Foin, Y. Huang, Materials technology in drug eluting balloons: current and future perspectives, *J. Contr. Release* 239 (2016) 92–106.
- [16] W. Li, R.N. Terry, J. Tang, M.R. Feng, S.P. Schwendeman, M.R. Prausnitz, Rapidly separable microneedle patch for the sustained release of a contraceptive, *Nat. Biomed. Eng.* 3 (3) (2019) 220–229.
- [17] H. Zhu, J. Mah Jian Qiang, C.G. Wang, C.Y. Chan, Q. Zhu, E. Ye, Z. Li, X.J. Loh, Flexible polymeric patch based nanotherapeutics against non-cancer therapy, *Bioact. Mater.* 18 (2022) 471–491.
- [18] I.J. Choi, A. Kang, M.H. Ahn, H. Jun, S.K. Baek, J.H. Park, W. Na, S.O. Choi, Insertion-responsive microneedles for rapid intradermal delivery of canine influenza vaccine, *J. Contr. Release* 286 (2018) 460–466.
- [19] F. Lu, X. Zhang, M. Nie, Y. Xu, Y. Wang, L. Shang, Y. Zhao, Y. Zhao, Photothermal responsive microspheres-triggered separable microneedles for versatile drug delivery, *Adv. Funct. Mater.* 32 (2022), 2110746.
- [20] K. Lee, J. Lee, S.G. Lee, S. Park, D.S. Yang, J.J. Lee, A. Khademhosseini, J.S. Kim, W. Ryu, Microneedle drug eluting balloon for enhanced drug delivery to vascular tissue, *J. Contr. Release* 321 (2020) 174–183.
- [21] J.A. Anderson, S. Lamichhane, T. Vierhout, A. Sherman, D. Engebretson, K. Pohlson, T. Remund, P. Kelly, *In vitro* particulate and *in vivo* drug retention study of a novel polyethylene oxide formulation for drug-coated balloons, *J. Vasc. Surg.* 67 (5) (2018) 1537–1545.
- [22] S.S. Wang, S.W. Hu, Q.H. Zhang, A.X. Xia, Z.X. Jiang, X.M. Chen, Mesenchymal stem cells stabilize atherosclerotic vulnerable plaque by anti-inflammatory properties, *PLoS One* 10 (8) (2015), e0136026.
- [23] Y. Chen, Y. Zeng, X. Zhu, L. Miao, X. Liang, J. Duan, H. Li, X. Tian, L. Pang, Y. Wei, J. Yang, Significant difference between sirolimus and paclitaxel nanoparticles in anti-proliferation effect in normoxia and hypoxia: the basis of better selection of atherosclerosis treatment, *Bioact. Mater.* 6 (3) (2021) 880–889.
- [24] X. Xue, H. Zhang, H. Liu, S. Wang, J. Li, Q. Zhou, X. Chen, X. Ren, Y. Jing, Y. Deng, Z. Geng, X. Wang, J. Su, Rational design of multifunctional CuS nanoparticle-PEG composite soft hydrogel-coated 3D hard polycaprolactone scaffolds for efficient bone regeneration, *Adv. Funct. Mater.* (2022), 2202470.
- [25] M. Dziadek, K. Dziadek, K. Checinska, B. Zagrajczuk, M. Golda-Cepa, M. Bryzyczny-Wloch, E. Menaszek, A. Kopec, K. Cholewa-Kowalska, PCL and PCL/bioactive glass biomaterials as carriers for biologically active polyphenolic compounds: comprehensive physicochemical and biological evaluation, *Bioact. Mater.* 6 (6) (2021) 1811–1826.
- [26] D. Zhao, T. Zhu, J. Li, L. Cui, Z. Zhang, X. Zhuang, J. Ding, Poly(lactic-co-glycolic acid)-based composite bone-substitute materials, *Bioact. Mater.* 6 (2) (2021) 346–360.
- [27] Y. Kang, C. Xu, L. Meng, X. Dong, M. Qi, D. Jiang, Exosome-functionalized magnesium-organic framework-based scaffolds with osteogenic, angiogenic and anti-inflammatory properties for accelerated bone regeneration, *Bioact. Mater.* 18 (2022) 26–41.
- [28] D. Lee, S. Kwon, S.Y. Jang, E. Park, Y. Lee, H. Koo, Overcoming the obstacles of current photodynamic therapy in tumors using nanoparticles, *Bioact. Mater.* 8 (2022) 20–34.
- [29] C. Liu, Y. Cao, Y. Cheng, D. Wang, T. Xu, L. Su, X. Zhang, H. Dong, An open source and reduce expenditure ROS generation strategy for chemodynamic/photodynamic synergistic therapy, *Nat. Commun.* 11 (1) (2020) 1735.
- [30] M. Li, X. Sun, N. Zhang, W. Wang, Y. Yang, H. Jia, W. Liu, NIR-activated polydopamine-coated carrier-free “Nanobomb” for in situ on-demand drug release, *Adv. Sci.* 7 (7) (2018), 1800155.
- [31] S. Steiner, A. Schmidt, T. Zeller, G. Tepe, M. Thieme, L. Maiwald, H. Schröder, W. Euringer, M. Ulrich, K. Brechtel, S. Brucks, E. Blessing, J. Schuster, R. Langhoff, S. Schellong, N. Weiss, D. Scheinert, Compare: prospective, randomized, non-inferiority trial of high- vs. low-dose paclitaxel drug-coated balloons for femoropopliteal interventions, *Eur. Heart J.* 41 (27) (2020) 2541–2552.
- [32] A. Boitet, S. Grassin-Delyle, L. Louedec, S. Dupont, E. Lamy, M. Coggia, J.B. Michel, R. Coscas, An experimental study of paclitaxel embolisation during drug coated balloon angioplasty, *Eur. J. Vasc. Endovasc.* 57 (4) (2019) 578–586.
- [33] X. Ning, C. Wiraja, W.T.S. Chew, C. Fan, C. Xu, Transdermal delivery of Chinese herbal medicine extract using dissolvable microneedles for hypertrophic scar treatment, *Acta Pharm. Sin. B* 11 (9) (2021) 2937–2944.
- [34] Q. Zhang, L. Shi, H. He, X. Liu, Y. Huang, D. Xu, M. Yao, N. Zhang, Y. Guo, Y. Lu, H. Li, J. Zhou, J. Tan, M. Xing, G. Luo, Down-regulating scar formation by microneedles directly via a mechanical communication pathway, *ACS Nano* 16 (7) (2022) 10163–10178.
- [35] Q. Li, R. Xu, H. Fan, J. Xu, Y. Xu, P. Cao, Y. Zhang, T. Liang, Y. Zhang, W. Chen, Z. Wang, L. Wang, X. Chen, Smart mushroom-inspired imprintable and lightly detachable (MILD) microneedle patterns for effective COVID-19 vaccination and decentralized information storage, *ACS Nano* 16 (5) (2022) 7512–7524.
- [36] T.B. Thomsen, C.J. Hunt, A.S. Meyer, Influence of substrate crystallinity and glass transition temperature on enzymatic degradation of polyethylene terephthalate (PET), *N. Biotech.* 69 (2022) 28–35.
- [37] J.F. Granada, M. Ferrone, G. Melnick, L. Crookall, D. Schulz-Jander, S. Tunev, R. J. Melder, G.L. Kaluza, Downstream paclitaxel released following drug-coated balloon inflation and distal limb wound healing in swine, *JACC Basic Transl. Sci.* 6 (5) (2021) 416–427.

- [38] K.J. Rocha-Singh, The ranger “low-dose” paclitaxel drug-coated balloon: is less really more? *Jacc-Cardiovasc. Inte.* 14 (10) (2021) 1134–1136.
- [39] A.M. Chopra, A. Rapkiewicz, R. Daggubati, A. Sequeira, Y.C. Hu, D.L. Bhatt, S. K. Sharma, J.P. Cruz, A.R. Tzafirri, E.R. Edelman, Analysis: intravascular devices with a higher risk of polymer emboli: the need for particulate generation testing, *Biomed. Instrum. Technol.* 54 (1) (2020) 37–43.
- [40] S.Y. Lee, M.K. Hong, D.H. Shin, J.S. Kim, B.K. Kim, Y.G. Ko, D. Choi, Y. Jang, Mechanisms of postintervention and nine-month luminal enlargement after treatment of drug-eluting in-stent restenosis with a drug-eluting balloon, *Am. J. Cardiol.* 113 (9) (2014) 1468–1473.
- [41] I. Rykowska, I. Nowak, R. Nowak, Drug-eluting stents and balloons-materials, structure designs, and coating techniques: a review, *Molecules* 25 (20) (2020) 4624.
- [42] H. Kamada, H. Kobara, H. Yamana, N. Fujita, D. Namima, T. Kohno, M. Hirata, R. Nakabayashi, K. Okano, T. Masaki, Repeated balloon inflation under low pressure may reduce serious adverse events during endoscopic papillary large balloon dilation, *J. Hepato-Bil-Pan Sci.* 29 (5) (2022) e33–e35.
- [43] T. Zhang, G. Guo, L. Yang, Y. Wang, An ultralow dose paclitaxel coated drug balloon with an outer protective sheath for peripheral arterial disease treatment, *J. Mater. Chem. B* 9 (10) (2021) 2428–2435.
- [44] M. Ceresnakova, D. Murray, T. Soulimane, S.P. Hudson, Candidates for smart cardiovascular medical device coatings: a comparative study with endothelial and smooth muscle cells, *Eur. J. Pharmacol.* 910 (2021), 174490.
- [45] J. Lindman, M.M. Khammy, P.R. Lundegaard, C. Aalkjær, T.A. Jepps, Microtubule regulation of Kv7 channels orchestrates cAMP-mediated vasorelaxations in rat arterial smooth muscle, *Hypertension* 71 (2) (2018) 336–345.
- [46] S. Bettink, M. Löchel, D. Peters, W. Haider, U. Speck, B. Scheller, Efficacy and safety of a magnesium stearate paclitaxel coated balloon catheter in the porcine coronary model, *Int. J. Cardiol.* 331 (2021) 46–56.
- [47] C. Song, C. Zhou, J. Zhang, X. Feng, X. Cui, F. Zhang, J. Ma, E.S. Toft, J. Ge, H. Zhang, Ultrasound controlled paclitaxel releasing system-A novel method for improving the availability of coronary artery drug coated balloon, *Cathet. Cardiovasc. Interv.* 96 (2) (2020) e119–e128.
- [48] E. Yamamoto, S. Watanabe, B. Bao, H. Watanabe, K. Nakatsuma, M. Izuhara, K. Ono, G. Nakazawa, T. Kimura, N. Saito, Preclinical evaluation of a paclitaxel-incorporated nanoparticle-coated balloon in rabbit and porcine models, *Cardiovasc. Revascula.* 19 (4) (2018) 433–437.
- [49] K. Lee, S.G. Lee, I. Jang, S.H. Park, D. Yang, I.H. Seo, S.K. Bong, D.H. An, M.K. Lee, I.K. Jung, Y.H. Jang, J.S. Kim, W. Ryu, LinearS micro-patterned drug eluting balloon (LMDEB) for enhanced endovascular drug delivery, *Sci. Rep.* 8 (1) (2018) 3666.
- [50] P.P. Buszman, K. Milewski, A. Zurakowski, J. Pajak, M. Jelonek, P. Gasior, A. Peppas, A. Tellez, J.F. Granada, P.E. Buszman, Experimental evaluation of pharmacokinetic profile and biological effect of a novel paclitaxel microcrystalline balloon coating in the iliofemoral territory of swine, *Cathet. Cardiovasc. Interv.* 83 (2) (2014) 325–333.
- [51] P.P. Buszman, A. Tellez, M.E. Afari, A. Peppas, G.B. Conditt, S.D. Rousselle, J. C. McGregor, M. Stenoien, G.L. Kaluza, J.F. Granada, Tissue uptake, distribution, and healing response after delivery of paclitaxel via second-generation iopromide-based balloon coating: a comparison with the first-generation technology in the iliofemoral porcine model, *JACC-Cardiovasc. Inte.* 6 (8) (2013) 883–890.
- [52] W. Kempin, S. Kaule, T. Reske, N. Grabow, S. Petersen, S. Nagel, K.P. Schmitz, W. Weitschies, A. Seidlitz, In vitro evaluation of paclitaxel coatings for delivery via drug-coated balloons, *Eur. J. Pharm. Biopharm.* 96 (2015) 322–328.
- [53] Z.Q. Zhang, Y.X. Yang, J.A. Li, R.C. Zeng, S.K. Guan, Advances in coatings on magnesium alloys for cardiovascular stents – a review, *Bioact. Mater.* 6 (12) (2021) 4729–4757.
- [54] C. Chen, J. Chen, W. Wu, Y. Shi, L. Jin, L. Petrini, L. Shen, G. Yuan, W. Ding, J. Ge, E.R. Edelman, F. Migliavacca, *In vivo* and *in vitro* evaluation of a biodegradable magnesium vascular stent designed by shape optimization strategy, *Biomaterials* 221 (2019), 119414.